NANO LETTERS

2007
Vol. 7, No. 6
1680−1685

Detecting SNPs Using a Synthetic Nanopore

Q. Zhao, G. Sigalov, V. Dimitrov, B. Dorvel, U. Mirsaidov, S. Sligar, A. Aksimentiev, and G. Timp*

Beckman Institute, University of Illinois, Urbana, Illinois 61801

Received March 21, 2007

ABSTRACT

We have discovered a voltage threshold for permeation through a synthetic nanopore of dsDNA bound to a restriction enzyme that depends on the sequence. Molecular dynamic simulations reveal that the threshold is associated with a nanonewton force required to rupture the DNA–protein complex. A single mutation in the recognition site for the restriction enzyme, i.e., a single nucleotide polymorphism (SNP), can easily be detected as a change in the threshold voltage. Consequently, by measuring the threshold voltage in a synthetic nanopore, it may be possible to discriminate between two variants of the same gene (alleles) that differ in one base.

Restriction enzymes are used prevalently in recombinant DNA technology for cleaving double-helical DNA segments containing a specific target sequence. Another use is genotyping. Because the binding to the target is extraordinarily sequence specific, restriction enzymes can be used to identify single nucleotide polymorphisms (SNPs) that occur when variants of the same gene (alleles) differ in one base.

We have discovered a method for discriminating between alleles that uses a synthetic nanopore to measure the binding of a restriction enzyme to DNA. When a voltage is applied across a membrane containing a nanopore, polyanionic DNA immersed in electrolyte at the cathode diffuses toward the anode and is driven across the membrane by the electric field in the pore. The force due to the field acting on the strand during the translocation impels DNA to bend and stretch within the pore.[1−4] At low fields $\mathcal{E} < 500$ mV/10 nm, double-stranded DNA (dsDNA) easily permeates pores with diameters ≥ 2.4 nm because the double helix ($\sim$2 nm diameter) is smaller than the pore.[5] But the permeability of DNA through the pore changes dramatically if it is bound to a restriction enzyme.

To study the binding of a restriction enzyme like *Eco*RI to DNA, we introduced an excess of the enzyme in solution with DNA without the Mg^{+2} cofactor that is required for cleaving the nucleic acid. Under these conditions, *Eco*RI is thought to bind and diffuse along DNA.[6,7] The diffusive motion along the strand is arrested at the cognate site, i.e., −GAATTC− for *Eco*RI. Bulk measurements of the binding at the cognate site indicate a free energy of formation $\Delta G = -15.2$ kcal/mol.[6−9] However, the introduction of any mutation among the cognate sites produces a position-dependent reduction in the binding energy that ranges from 6−13 kcal/mol.[8,9] Site-specific DNA-binding proteins also have an affinity for nonspecific DNA. In contrast with site-specific binding or binding to a noncognate site with a single nucleotide mutation, a nonspecifically bound complex is not localized to a particular site. For *Eco*RI, sites that differ from the cognate sequence by two or more base pairs (bp) are considered nonspecific because they are not cleaved and show low binding constants. For a nonspecifically bound *Eco*RI−DNA complex, the free energy of formation is reduced to −4.8 kcal/mol.[8,9]

We measured the permeability of dsDNA in solution with *Eco*RI through nanometer-diameter pores in nominally 10 nm thick Si_3N_4 membranes as a function of the applied voltage. With an enzyme−DNA complex trapped in the nanopore, the electric field in the pore pulls on the DNA, introducing a shear force between the enzyme and the cognate sites in DNA. We observe a threshold in the field required to rupture the bond that depends on the sequence and enzyme. Molecular dynamics (MD) simulations reveal that the rupture occurs within several nanoseconds with a force $\sim$1 nN.

The fabrication of the synthetic nanopores in inorganic membranes has been described elsewhere.[10] A single nanopore is created in a Si_3N_4 membrane by stimulated decomposition and sputtering using a tightly focused electron beam as small as 0.5 nm (Gaussian width) in diameter in a JEOL 2010F transmission electron microscope (TEM) operating at 200 keV. Figure 1a shows transmission electron micrographs (TEM) of three pores in Si_3N_4 membranes nominally 10 nm thick. The pores are 1.8 nm × 2.5 ± 0.2 nm (blue); 2.4 nm × 3.2 ± 0.2 nm (green), and 3.6 ± 0.2 nm (red) in diameter; the shot noise observed in the area identified as the pore is indicative of perfect transmission

* Corresponding author. E-mail: gtimp@uiuc.edu.

10.1021/nl070668c CCC: $37.00
Published on Web 05/15/2007

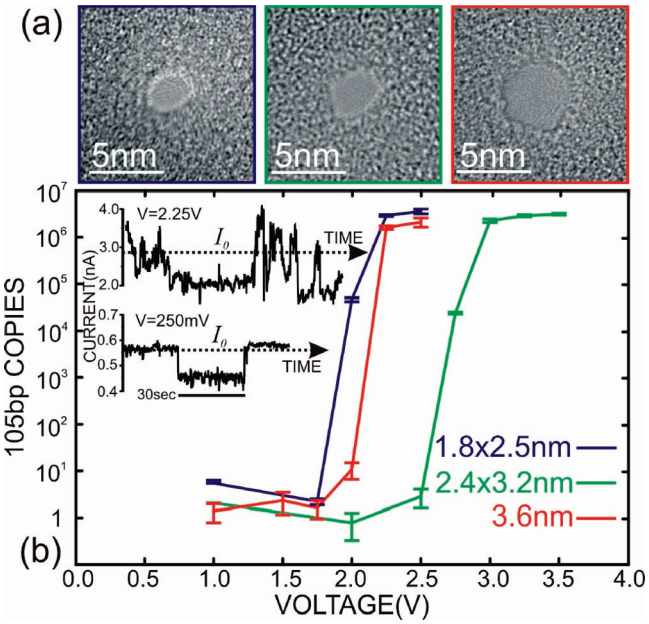

Figure 1. Threshold voltage depends on pore diameter. (a) TEM micrographs taken at a tilt angle of 0° of three nanopores, 1.8 nm × 2.5 nm (blue), 2.4 nm × 3.2 nm (green), and 3.6 nm (red) diameter, sputtered with a tightly focused high-energy electron beam in nominally 10 nm thick Si_3N_4 membranes. The shot noise observed in the area identified as the pore is indicative of perfect transmission of the electron beam through the membrane. A 105 bp permeates these pores only for $V > 1.75$ V. (b) qPCR results indicating the number of 105 bp DNA copies from *Eco*RI−DNA complex that permeates the membrane through the pores in (a) found at the positive (+) electrodes in a bi-cell as a function of the voltage across the membrane. The inset shows the electrolytic current through the 2.4 nm × 3.2 nm pore as a function of time with the membrane voltage as a parameter. Long duration transients >10 s and transient currents greater than the open pore current $>I_0$ are observed.

of the electron beam through the membrane. The thickness of similarly processed 10 nm membranes was inferred from TEM to be 12 ± 2 nm, which is consistent with result 12 ± 3 nm obtained from using electron energy loss spectroscopy. The TEM images shown in Figure 1 represent a two-dimensional projection through the membrane. To investigate the three-dimensional structure, we tilted the membrane in the specimen about the pore axis and explored various defocus conditions. We have developed models for the pore geometry. Although it is not unique, a simple model for the three-dimensional structure of the pore consists of two intersecting cones each with a cone angle of ~10°.[10]

To further characterize the pore, we measured the electrolytic current as a function of the electrochemical potential applied across the membrane at 23.5 ± 1°C. All experiments were carried out in a membrane transport bi-cell made from acrylic using silicone O-rings with PDMS coatings to seal the membrane to the acrylic (with >5.0 ± 0.2 TΩ resistance.) The membrane separates two reservoirs: one with a 140 μL volume on the cis side, and the other on the trans side with 15 mL volume. Each reservoir contains a Ag/AgCl electrode, which is connected to an Axopatch 200B amplifier used in resistive feedback mode. LabView software is used to record the ionic current and to apply the voltage across the membrane. All data is low-pass filtered at 10 kHz and digitized at 50 kHz for analysis. The current−voltage (I−V) characteristics of the pores shown in Figure 1a were measured over a range of ±1 V in microfiltered buffered 100 mM KCl (10 mM Tris, pH 8.0) after >55 h of immersion in deionized water. The characteristics are approximately linear; line fits to the data yield the conductances: 89.5 ± 3 pS for the 1.8 nm × 2.5 ± 0.2 nm (blue) pore, 0.49 ± 0.03 nS for the 2.4 nm × 3.2 ± 0.2 nm (green) pore, and 1.46 ± 0.03 nS for the 3.6 ± 0.2 nm (red) pore shown in Figure 1a, and 1.18 ± 0.03 nS for 3.4 nm × 4.7 nm pore shown in Figure 3a and 2.12 ± 0.03 nS for the 3.4 nm × 4.5 nm pore shown in Figure 3b. It is apparent that the conductance does not scale linearly with the diameter derived from TEM.[10−12] We have analyzed similar measurements using molecular dynamics to estimate the ion mobility and then solving coupled Poisson−Nernst−Planck and the Stokes equations self-consistently for the ion concentration, velocity, and electrical potential. We find that the measurements are consistent with the presence of a small (relative to DNA) fixed negative charge in the pore and a reduction of the ion mobility due to the fixed charge and the ion proximity to the pore wall.[10]

Following the conductance measurements, we tested the permeability of dsDNA in solution with *Eco*RI through nanometer-diameter pores of Figure 1 as a function of the applied voltage. We used two separate dsDNA strands:

1. A 105 bp dsDNA, which is extracted from the pUC19 (NEB part no. N3041S) vector with the sequence: 5′-TAAGT TGGGT AACGC CAGGG TTTTC CCAGT CACGA CGTTG TAAAA CGACG GCCAG TGAAT TC*GAG CT*CGG TACCC GG*GGA TCC*TC TAGAG TCGAC CTGCA GGCAT-3′ where the cognate site for *Eco*RI is highlighted with an underline (and sites with double substitutions are indicated in italics).

2. A 900 bp DNA strand, which is extracted from a pTWIN1 vector (NEB part no. N6951S) using forward primer GAATGACATCATTGTACACA and reverse primer GCCAACTCAGCTTCCTTTCG to amplify a sequence that spans both *Eco*RI and *Bam*HI cognates; the length between the start of the *Eco*RI recognition site and start of *Bam*HI site is 815 bp. Selected portions of the sequence are given below: GAATGACATCATTGTACACAACGGAAGAGCCATGGGCGGCCGCGAATTCCTCGAGGGCTCTTCCTGCATCACGGGAGATGCACTAGTTGCCCTACCCGAGGGCGAGTCGGTACGCATCGCCGACATCGTGCCGGGTGCGCGGCCCAACAGTGACAACGCCATCGACCTGAAAGTCCTTGACCGGCATGGCAATCCCGTGCTCGCCGACCGGCTGTTCCACTCCGGCGAGCATCCGGTGTACACGGTGCGTACGGTCGAAGGTCTGCGTGTGACGGGCACCGCGAACCACCCGTTGTTGTGTTTGGTCGACGTCGCCGGGGTGCCGACCCTGCTGTGGAAGCTGATCGACGAAATCAAGCCGGGCGATTACGCGGTGATTCAACGCAGCGCATTCAGCGTCGACTGTGCAGGTTTTGCCCGCGGAAAACCCGAATTTGCGCCCACAACCTACACAGTCGGCGTCCCTGGACTGGTGCGTTTCTTGGAAGCACACCACCGAGACCCGGACGCCCAAGCTATCGCCGACGAGCTGACCGACGGGCGGTTCTACTACGCGA-

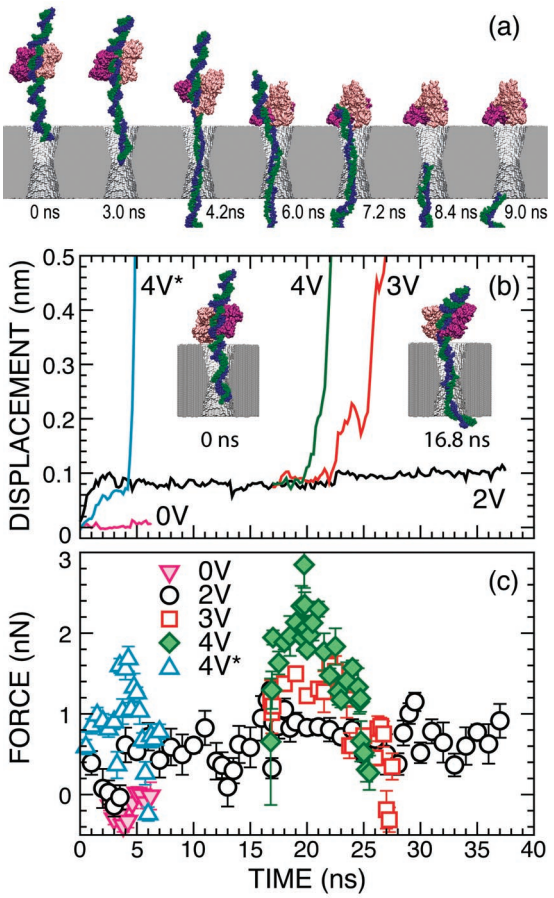

Figure 2. MD simulations of *Eco*RI−DNA complex encountering synthetic nanopore. (a) Snapshots illustrating simulated dissociation of an *Eco*RI−DNA complex due to the electric field in a nanopore. The Si_3N_4 membrane is shown in gray, two strands of DNA in blue and green, a protein dimer in pink and purple, water and ions are not shown. Time elapsed from the moment a 4 V transmembrane bias was applied is indicated. (b) The protein−DNA displacement vs time in four MD simulations carried out at different transmembrane biases. The displacement is defined as the change of the contact distance between the cognate nucleotides and the binding site of *Eco*RI. The insets illustrate the starting (0 ns) and the midway (16.8 ns) conformations of the *Eco*RI−DNA complex in a simulation carried out at a 2 V bias. Two additional simulations, at 3 and 4 V, were initiated starting from the midway conformation of the 2 V simulation. Another simulation at 4 V (denoted as 4 V*) began from a different conformation and is illustrated in (a). (c) The effective force of the DNA−protein interaction, defined as a sum of all nonbonded forces acting at the 12 bp DNA fragment adjacent to the protein. The effective force plots correspond to the displacement plots shown in (b), color-coded accordingly. Each data point was obtained by averaging the instantaneous force over 8−25 ps; the error bars are the standard errors of the mean.

AAGTCGCCAGTGTCACCGACGCCGGCGTGCAGCCG-GTAGCCTTCGTGTCGACACGGCAGACCACGCGTTT-ATCACGAACGGGTTCGTCAGCCACGCTACTGGCCT-CACCGGTCTGAACTCAGGCCTCACGACAAATCCTGG-TGTATCCGCTTGGCAGGTCAACACAGCTTATACTG-CGGGACAATTGGTCACATATAACGGCAAGACGTATA-AATGTTTGCAGCCCCACACCTCCTTGGCAGGATGG-GAACCATCCAACGTTCCTGCCTTGTGGCAGCTTCA-ATGACTGCAGGAAGG**GGATCC**GGCTGCTAACAAA-GCCCGAAAGGAAGCTGAGTTGGC where the cognate site for *Eco*RI is highlighted with an underline, while the site for *Bam*HI is highlighted in bold.

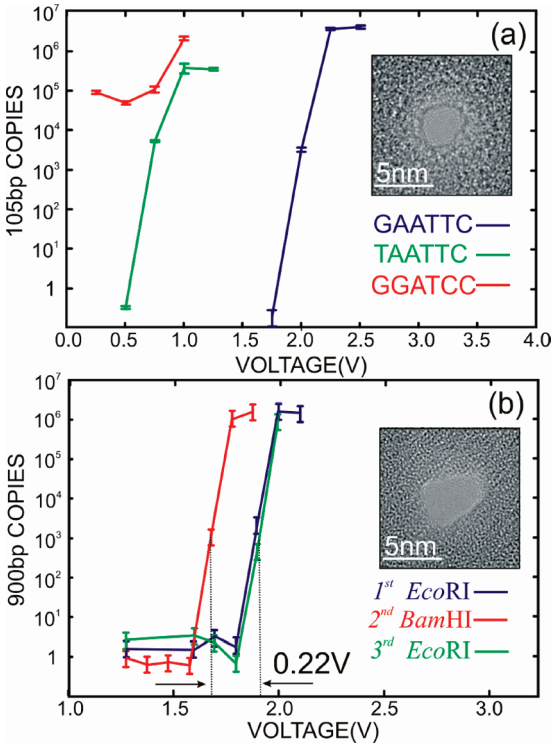

Figure 3. Threshold voltage depends on sequence and the enzyme. (a) qPCR results indicating that the number of 105 bp copies from *Eco*RI−DNA that permeates a pore with a threshold voltage that depends on the DNA sequence. The inset shows a TEM micrograph of the a 2.7 nm × 3.4 nm pore. The cognate sequence GAATTC (blue) has a threshold voltage of about 1.5 V, but in constrast, with a substitution for the first-base, TAATTC (green) corresponding to star activity has a threshold of only 0.5 V. There is no threshold apparent for the two-base substitution GGATCC (red), which is associated with nonspecific binding. (b) qPCR results indicating that the number of 900 bp DNA copies from either *Eco*RI−DNA or BamHI−DNA that permeates a pore depends on the enzyme. The inset shows a TEM micrograph of the 3.4 nm × 4.5 nm pore. The threshold for the *Eco*RI and *Bam*HI rupture scales with the bulk dissociation energies.

A membrane including a pore was mounted in a bi-cell, and then either *Eco*RI or *Bam*HI in solution with DNA containing the cognate sequence was injected into the electrolyte at the cathode. We introduce either commercial grade *Eco*RI (100 000 U/mL stock concentration, 62 kD dimer, 2×10^6 U/mg specific activity; (NEB part no. R0101Q) or *Bam*HI (100 000 units/mL, 52 kD dimer, 1.7×10^6 U/mg specific activity; (NEB part no. R0136Q) without purification into the cis chamber of the membrane bi-cell. To a solution containing microfiltered 100 mM KCl and10 mM Tris, we added HCl to adjust the pH value to 7.9. The 100 mM KCl electrolyte concentration was chosen because *Eco*RI has a tendency to aggregate at lower ionic strengths.[2] We then mixed 400 μL of this buffer with 40 μL of *Eco*RI (or *Bam*HI) solution and 2 μL of 105 bp DNA solution (diluted to 88 pg/μL for 105 bp, and 10 ng/μL for 900 bp) and incubated at 37 °C for 10 h to ensure that the enzyme binds to the DNA. None of the buffers contained Mg^{2+}, which is required for catalytic activity of the restriction

endonucleases. The solution injected into the cis reservoir of the bi-cell showed pH 7.9.

With a voltage applied across the membrane, we observed an electrolytic current through the pore. Superimposed on the open pore current, I_0, we detected transients associated with the *Eco*RI−DNA complex interacting with the pore, as illustrated in the inset to Figure 1b. We have previously reported[11,12] that electric-field-driven translocations of unbound DNA cause temporary blockades of I_0, but the duration of the transients was generally short (<100 ms). In contrast, we observe transients >10 s associated with the *Eco*RI−DNA, which is unprecedented for a synthetic pore. The translocation velocity of unbound DNA in a synthetic pore is estimated to be >1 bp/ns at these voltages,[3,4,11,13] so the duration of these events must represent an extended residence time of the complex over the pore that terminates either through dissociation and subsequent translocation of the DNA or with the complex uneventfully exiting the pore due to thermal agitation. The same inset also shows transient currents greater than the open pore current. Currents $>I_0$ have been observed before[11,13,14] and are attributed to a local enrichment of electrolyte near the pore due to counter ions responding to the molecular charge. The narrow bandwidth (10−100 kHz) of the current amplifier we used precludes the observation of transients shorter than 10−100 μs. Hence, to establish unequivocally if DNA injected at the cathode permeates the membrane through the pore, the DNA near the anode was analyzed using quantitative PCR (qPCR).

A PCR reagent system obtained from Invitrogen (Carlsbad, CA) was used in conjunction with the sequence-specific primers synthesized by IDT−DNA (Ames, IA) to amplify the DNA, which was analyzed by agarose gel electrophoresis. Finally, we used a Qiagen gel extraction kit to purify the DNA and remove primers, nucleotides, enzymes, salts, agarose, ethidium bromide, and other impurities. The final solution from the extraction had a concentration of about 44 ng/μL for the 105 bp and 10 ng/μL for the 900 bp.

We systematically investigated DNA permeability through nanopores in the membrane as a function of pore diameter. Corresponding to the gel arrays shown in the Supporting Information, Figure 1b represents the results of three qPCR analyses showing the number of DNA copies permeating as a function of the applied potential. SYBR Green I, a commonly used fluorescent DNA binding dye, was included in the qPCR reaction mix. SYBR Green I binds all dsDNA and the increase in fluorescence of it can be detected after each PCR cycle, which is proportional to the amount of DNA.

Figure 1b illustrates DNA permeability through the three pores shown in Figure 1a as a function of the voltage. When the diameter is small enough to preclude the translocation of the complex, while at the same time allowing DNA to easily permeate the membrane through the pore ($2.4 < d <$ 4.9 nm, see Supporting Information), we observe a voltage threshold for permeation of dsDNA that depends on the pore. Apparently, dsDNA can be forced through the pores only if the voltage is $V > 1.75$ V, which corresponds to an electric field $\mathcal{E} > 2.1 \pm 0.2$ MV/cm that is estimated by assuming a cylindrical pore geometry and a uniform voltage drop. The threshold must depend on either the geometry or charge in the pore[10] because the thresholds for the 1.8 nm × 2.5 nm and 3.6 nm pores are comparable, while the threshold for the 2.4 nm × 3.2 nm pore is $V > 2.5$ V.

Assuming that the bound protein frustrates DNA permeability through the pore, a large force corresponding to ΔG will be required to dissociate the complex and induce the translocation of DNA. To investigate the microscopic mechanics of the rupture and assess the forces involved, we used MD to simulate the rupture of the complex under the influence of an applied voltage. A microscopic model of an *Eco*RI−DNA complex was built based on a 0.18 nm resolution crystal structure (Protein Data Bank code 1CKQ).[15] The first 15 residues of the protein not resolved in the X-ray structure were not modeled. The 12 bp fragment of DNA resolved in the X-ray structure (CGCGAATTCGCG) was extended to 62 bp by adding two pre-equilibrated DNA fragments (20 and 30 bp long) to the ends of the resolved fragment. A Si_3N_4 membrane was built by replicating a unit cell of β-Si_3N_4 crystal to form a 10.3 nm thick hexagonal prism of a 117.23 nm^2 cross-section. A 2.7 nm diameter double-cone pore was produced by removing silicon and nitrogen atoms. The surface of Si_3N_4 was modified to produce a uniform surface charge of 100 mC/m^2 (about 0.6 e/nm^2).[10] The Si_3N_4 structure was merged with the *Eco*RI−DNA complex, having the DNA molecule oriented perpendicular to the membrane and its longer tail inserted by 2.6 nm (system I) or 8.6 nm (system II) into the pore. The resulting structures were then solvated in a volume of pre-equilibrated TIP3P water molecules. Potassium and chlorine ions were added, corresponding to a concentration of 0.1 M. The final systems included about 415 000 atoms. To build a system for SMD simulations (system III), the 12 bp DNA fragment resolved in the X-ray structure was extended to 34 bp by adding 11 bp to either end of the resolved fragment. The *Eco*RI−DNA complex was then solvated in 100 mM aqueous solution of KCl. The final system measured 12 × 12 × 18 nm^3 and included about 248 000 atoms.

Each system constructed underwent 2000 steps of minimization followed by gradual heating from 0 to 295 K in 4 ps. Systems I and II were equilibrated in the *NPT* ensemble (i.e., with particle number N, pressure P, and temperature T fixed) for 1 ns each, having all backbone atoms of *Eco*RI−DNA restrained. System III underwent 8.4 ns equilibration. For the first 2.2 ns, all backbone atoms of *Eco*RI−DNA were restrained, while in the rest 6.2 ns only α-carbons of the protein were subject to weak harmonic restraints (k_{spring} = 10 kcal/(mol nm^2)).

Our MD simulations were performed using the program NAMD2,[16] periodic boundary conditions, particle mesh Ewald full electrostatics and multiple time stepping,[17] the CHARMM27[18] force field describing DNA, protein, water, and ions, and a custom force field describing the Si_3N_4 membrane.[1,13] The integration time step chosen was 1 fs. The equilibration in the *NPT* ensemble was performed using the Nosé−Hoover−Langevin piston pressure control.[19] Van der Waals energies were calculated using a smooth (1−1.2

nm) cutoff. During the equilibration, the temperature was kept at 295 K by applying Langevin forces[19] to all heavy atoms; the Langevin damping constant was set to 5 ps^{-1}, and the backbone atoms of the *Eco*RI−DNA complex were restrained by applying harmonic forces with the spring constant of 100 kcal/(mol nm^2) unless stated otherwise. Other simulation conditions and protocols are described in Aksimentiev et al.[13] To simulate an electric-field-driven rupture of an *Eco*RI−DNA complex, a uniform electric field was applied to all atoms in systems I and II. Inducing this field rearrangement of ions and water focused the electric field to the vicinity of the membrane and produced a transmembrane bias equivalent to $-E \cdot L$, where L is the system size in the direction of the applied field (in our case, normal to the Si_3N_4 membrane).[13] All simulations under an external electric field were carried out in the *NVT* (constant *N*, volume *V*, and *T*) ensemble. The damping constant of the Langevin thermostat was set to 1 ps^{-1}.

All SMD simulations were carried out on system III according to standard protocols.[20−22] A harmonic restraint, applied to the center of mass of a terminal 10 bp DNA fragment (k_{spring} = 50 000 kcal/(mol nm^2)), was moved with a constant velocity away from *Eco*RI in the direction of the DNA end. Each α-carbon of *Eco*RI was harmonically restrained using a weak spring (k_{spring} = 10 kcal/(mol nm^2)).

The displacement of the 6 bp cognate fragment from its equilibrium position in the *Eco*RI−DNA complex was calculated using the following algorithm. First, we identified all atom pairs (*ij*) such that, in each pair, atom *i* belonged to a cognate nucleotide and atom *j* belonged to the protein, and their distance $\langle d_{ij} \rangle$, averaged over the 6.2 ns equilibration of system III, did not exceed 0.4 nm. This procedure yielded 80 such atom pairs, 40 for each DNA strand. Next, for each pair, the distance d_{ij} was computed along the simulated trajectory. Finally, the displacement of the cognate sequence from its binding pocket in *Eco*RI was determined as an average change of the pair distance, i.e., $R = \sum_{ij} (d_{ij} - \langle d_{ij} \rangle)/n$, where $n = 80$.

The effective force between DNA and *Eco*RI in the nanopore simulations was determined by computing the total nonbonded force on the 12 bp DNA fragment adjacent to *Eco*RI. Using a custom version of the NAMD2 program, a sum of *all* van der Waals, short-range electrostatic (Coulomb), long-range electrostatic (PME), and the external electric field forces on the 12 bp DNA fragment were computed for every time step (1 fs) of a 25 ps postprocessing MD run, restarted from a conformation of interest. The instantaneous forces were averaged during the postprocessing run; the standard error of the mean was determined using 20 fs mean values of the force. All analysis and visualization were done using VMD.[23]

In the 9.6 ns MD simulation shown in Figure 2a, 4 V caused the complex to dissociate and induced the translocation of DNA. On the other hand, no rupture was observed in a 38 ns simulation carried out at 2 V, as illustrated in Figure 2b. However, by restarting this simulation near the midpoint (16.8 ns) with both 3 V and 4 V, we were able to dissociate the complex. (The rupture occurred at 4 V sooner than at 3 V.) Figure 2c shows the force on the complex associated with the trajectories in (b). At 2 V, the force fluctuates around 0.7 nN, while at 3 V and 4 V, coinciding with the rupture of the complex, the force > 1.2 nN. In the Supporting Information, we show that the rupture force, f^*, depends logarithmically on the loading rate, r: i.e., $f^* = 1.710 + 0.364 \ln(r)$, and we conclude that, for loading rates from 0.1−1 N/s, the dissociation of the complex occurs in <10 ns with a force ∼1 nN. We find that rupture occurs when a ∼1 nN force stretches the bonds associated with the first two base pairs from the 5′ end in the 6 bp cognate site and an adjacent flanking nucleotide by more than $a \sim 0.15-0.2$ nm, such that $\Delta G = f^* a \sim 13-17$ kcal/mol.

We also find that threshold voltage depends on the DNA sequence. Figure 3a represents three qPCR analyses of the permeation of DNA variants bound to *Eco*RI. The pore used to test the permeability (see inset) is 2.7 nm × 3.4 ± 0.2 nm and the corresponding threshold for disrupting the bond between the *Eco*RI and the cognate sites on the DNA is V = 1.75 V. However, the threshold voltage collapses to V = 0.5 V, with a single base mutation from G to T on the first cognate site from the 5′ end, in correspondence with the change in the bulk dissociation energy for the same mutation. An estimate for the free energy of formation for the first-base substitution with −TAATTC− is −8.6 kcal/mol (with a different flanking sequence and strand length.)[6,8] The ratio of the bulk dissociation energies, 8.6/15.2, is comparable to the ratio of the thresholds, 0.5/1.75. For a two-base substitution among the cognate sites (the red trace in Figure 3a), the *Eco*RI−DNA bond is nonspecific, and correspondingly, we observe no threshold (i.e., V < 200 mV). From the ratio of the nonspecific bulk binding energy to the bulk dissociation energy for the cognate sites, we expect a threshold V < 500 mV.[8]

Restriction enzymes specific to hundreds of distinct sequences have been identified, and corresponding cognate sites can be found in almost any gene. Consequently, measurement of the threshold voltage might ultimately be used for genotyping DNA without sequencing it completely. However, the efficacy of using different enzymes will depend on the ability to discriminate between the threshold voltages. As a test, we measured the threshold for permeation through a nanopore of a longer strand of dsDNA (900 bp) that incorporates cognate sites for both *Eco*RI (GAATTC) as well as *Bam*HI (GGATCC). Because the respective cognate sites differ by two base pairs, we expect only nonspecific binding of one enzyme to the other site. Three qPCR analyses are shown in Figure 3b: the first measures the threshold associated with the *Eco*RI−DNA, the second measures the threshold for *Bam*HI−DNA, and the third measures *Eco*RI−DNA again to establish reproducibility. The inset shows the nanopore used for this test (3.4 nm × 4.5 ± 0.2 nm): it has a threshold voltage of V = 1.80 V for rupturing the *Eco*RI−DNA bond. Notice that the threshold for rupturing *Bam*HI−DNA complex is 220 mV lower, i.e., V = 1.58 V, and the ratio of the thresholds (1.58/1.80) corresponds to the ratio of the dissociation energies (13.2/15.2). The 220 mV

difference is easily resolved because a second measurement of *Eco*RI−DNA after measuring the *Bam*HI−DNA threshold reports the original threshold.

In summary, these results demonstrate a voltage threshold for permeation through a synthetic nanopore of dsDNA bound to a restriction enzyme that depends on the sequence and on the enzyme, a SNP in the recognition site can easily be detected. Because SNPs are used to predict susceptibility to various therapeutic regimes, and identify viral and bacterial infections, this simple detection strategy prospectively offers enough sensitivity to make single point-of-care diagnostics a reality.

Acknowledgment. We gratefully acknowledge the use of the Center for Microanalysis of Materials supported by the U.S. DOE grant DEFG02-91-ER45439 and the supercomputer time provided through the LRAC grant MCA05S028 and the Turing cluster (UIUC). The modified version of NAMD that was used to compute the rupture forces from MD simulations was developed by B. Luan and D. Wells. This work was funded by grants from NIH, R01 HG003713A and P41 RR05969.

Supporting Information Available: PCR/gel analysis, SMD analysis. This material is available free of charge via the Internet at http://pubs.acs.org.

References

(1) Heng, J. B.; Aksimentiev, A.; Ho, C.; Marks, P.; Grinkova, Y. V. ; Sligar, S.; Schulten, K.; Timp, G. *Biophys. J.* **2006**, *90*, 1098.
(2) Heng, J. B.; Aksimentiev, A.; Ho, C.; Marks, P.; Grinkova, Y. V. ; Sligar, S.; Schulten, K.; Timp, G. *Nano Lett.* **2005**, *5*, 1883.
(3) Storm, A. J.; Chen, J. H.; Zandbergen, H. W.; Dekker, C. *Phys. Rev. E* **2005**, *71*, 051903.
(4) Chen, P.; Gu, J.; Brandin, E.; Kim, Y.-R.; Wang, Q.; Branton, D. *Nano Lett.* **2004**, *4*, 2293.
(5) Saenger, W. *Principles of Nucleic Acid Structure*; Springer-Verlag: New York, 1984.
(6) Jen-Jacobsen, L. *Biopolymers* **1997**, *44*, 153.
(7) Jeltsch, A.; Alaves, J.; Wolfes, H.; Maas, G.; Pingoud, A. *Biochemistry* **1994**, *33*, 10215.
(8) Lesser, D. R.; Kurpiewski, M. R.; Jen-Jacobson, L. *Science* **1990**, *250*, 776.
(9) Jayaram, B.; McConnell, K. J.; Dixit, S. B.; Beveridge, D. L. *J. Comput. Phys.* **1999**, *151*, 333.
(10) Ho, C.; Qiao, R.; Heng, J.; Chatterjee, A.; Timp, R.; Aluru, N.; Timp, G. *Proc. Nat. Acad. Sci. U.S.A.* **2005**, *102*, 10445.
(11) Heng, J. B.; Ho, C.; Kim, T.; Timp, R.; Aksimentiev, A.; Grinkova, Y. V.; Sligar, S.; Schulten, K.; Timp, G. *Biophys. J.* **2004**, *87*, 2905.
(12) Siwy, Z. *Adv. Funct. Mater.* **2006**, *16*, 735; Siwy, Z.; Fuliński, A. *Phys. Rev. Lett.* **2002**, *89*, 198103.
(13) Aksimentiev, A.; Heng, J. B.; Timp, G.; Schulten, K. *Biophys. J.* **2004**, *87*, 2086.
(14) Chang, H.; Kosari, F.; Andreadakis, G.; Alam, M. A.; Vasmatzis, G.; Bashir, R. *Nano Lett.* **2004**, *4*, 1551.
(15) Horvath, M.; Rosenberg, J. M. Online resource: http://www.pdb.org/pdb/explore/explore.do?structureId=1CKQ, 1999.
(16) Phillips, J. C.; Braun, R.; Wang, W.; Gumbart, J.; Tajkhorshid, E.; Villa, E.; Chipot, C.; Skeel, R. D.; Kalé, L.; Schulten, K. *J. Comput. Chem.* **2005**, *26*, 1781.
(17) Batcho, P. F.; Case, D. A.; Schlick, T. *J. Chem. Phys*. **2001**, *115*, 4003.
(18) MacKerell, A. D., Jr.; Bashford, D.; Bellott, M.; Dunbrack, R. L., Jr.; Evanseck, J. D.; Field, M. J.; Fischer, S.; Gao, J.; Guo, H.; Ha, S.; Joseph-McCarthy, D.; Kuchnir, L.; Kuczera, K.; Lau, F. T. K.; Mattos, C.; Michnick, S.; Ngo, T.; Nguyen, D. T.; Prodhom, B.; Reiher, W. E., III; Roux, B.; Schlenkrich, M.; Smith, J. C.; Stote, R.; Straub, J.; Watanabe, M.; Wiórkiewicz-Kuczera, J.; Yin, D.; Karplus , M. *J. Phys. Chem. B* **1998**, *102*, 3586.
(19) Martyna, G. J.; Tobias, D. J.; Klein, M. L. *J. Chem. Phys*. **1994**, *101*, 4177.
(20) Brünger, A. T. *X-PLOR, version 3.1: A System for X-Ray Crystallography and NMR*; The Howard Hughes Medical Institute and Department of Molecular Byophysics and Biochemistry, Yale University: New Haven, CT, 1992.
(21) Grubmüller, H.; Heymann, B.; Tavan, P. *Science* **1996**, *271*, 997.
(22) Isralewitz, B.; Izrailev, S.; Schulten, K. *Biophys. J.* **1997**, *73*, 2972.
(23) Humphrey, W.; Dalke, A.; Schulten, K. *J. Mol. Graphics* **1996**, *14*, 33.

NL070668C